Strongly Localized Evanescent Optical Tamm States at Metal-DBR Interface

Xu-Lin Zhang, Jun-Feng Song, Xian-Bin Li, Jing Feng, and Hong-Bo Sun, *Member, IEEE*

***Abstract*—We study the eigenmodes of optical Tamm states (OTSs) at metal-distributed Bragg reflector interface. A peculiar type of non-propagating OTSs, named as evanescent OTSs, is found with mode propagation constant exhibiting the imaginary part to be much larger than the real part. The existence of such evanescent OTSs is attributed to the extension of Bragg forbidden band under complex propagation constants. An analytical solution of the evanescent OTSs is derived. Compared with propagating OTSs, transverse magnetic-polarized evanescent OTSs are found to exhibit more strongly localized field distributions associated with enhanced surface field intensity, which may be beneficial for surface-related applications such as sensing. Potential application as modulators is also demonstrated by using the nearly vertical dispersion characteristics around the transition wavelength between propagating OTSs and evanescent OTSs.**

***Index Terms*—Bragg forbidden band, effective refractive index, optical Tamm states, strongly localized field distributions.**

I. Introduction

ELECTROMAGNETIC surface waves are kind of states propagating along the interface between two different media with local maximum field intensity at the surface. Surface waves are directly involved in various surface-related applications, such as sensing [1], surface-enhanced Raman scatterings [2], etc. One of the well-known surface waves is surface plasmon polaritons (SPPs) [3]–[5], which can be excited through a prism or gratings as its wave vector is larger than that in the dielectric [6]–[8]. Recently, optical Tamm states (OTSs) have been developed at metal-distributed Bragg reflector (DBR) interface [9], [10] dielectric-DBR interface [11], [12], and two different DBRs interface [13], respectively. Besides, coupled OTSs [14]–[16] and applications for the control of spontaneous optical emission [17] and coupling with excitons [18], [19] have also been studied. In contrast to SPPs, both transverse magnetic (TM) and transverse electric (TE) polarized OTSs exist [9], [20]. Moreover, OTSs can be excited directly from free space incidence without the assistance of a prism or gratings. However, the mode localization characteristics of OTSs are much worse than those of SPPs [9]. Strongly localized field distributions are beneficial for surface-related applications such as sensing because of the enhanced surface field intensity [21]. Therefore, new types of OTSs are required to be studied in order to find strongly localized OTSs for these applications.

In this work we apply the optical waveguide mode theory to study the eigenmodes of OTSs at metal-DBR interface. A peculiar type of OTSs is for the first time found with its mode propagation constant exhibiting the imaginary part to be much larger than the real part. We name these OTSs as evanescent OTSs as they can be excited by evanescent incidence. An analytical solution of the evanescent OTSs is derived. The existence of such evanescent OTSs is a result of the extension of Bragg forbidden band under complex propagation constants. Compared with propagating OTSs, the TM-polarized evanescent OTSs are found to exhibit more strongly localized field distributions. Potential applications of the evanescent OTSs are also discussed in the paper.

Manuscript received December 31, 2012; revised February 19, 2013; accepted March 25, 2013. Date of publication March 29, 2013; date of current version April 12, 2013. This work was supported in part by NSFC (Grant Nos. 90923037, 61137001, 61107024, and 61177090).

The authors are with State Key Laboratory on Integrated Optoelectronics, College of Electronic Science and Engineering, Jilin University, Changchun 130023, China (e-mail: songjf@ime.a-star.edu.sg; hbsun@jlu.edu.cn).

Digital Object Identifier 10.1109/JLT.2013.2255583

II. Results and Discussions

A. Evanescent OTSs at Metal-DBR Interface

We study OTSs at a metal-DBR interface as shown in the inset of Fig. 1(a), where 50 bilayers of DBR are sandwiched by semi-infinite Ag layer and air layer. The structure parameters are chosen as $n_1 = 3.7$, $n_2 = 3$, $d_1 = 83.8$ nm, $d_2 = 103.3$ nm, and period $\Lambda = 187.1$ nm, with the quarter wave condition $n_1 d_1 = n_2 d_2$ satisfied. These parameters are the same as those applied in [9]. We consider the whole structure as a waveguide and apply the waveguide mode theory based transfer matrix method to solve the eigenmodes of this waveguide [22]. More specifically, the procedure is first to solve the scalar Helmholtz equation in each layer, which is $\partial^2 H_y/\partial x^2 + (k_0^2\varepsilon - \beta^2)H_y = 0$ for TM polarization and $\partial^2 E_y/\partial x^2 + (k_0^2\mu - \beta^2)E_y = 0$ for TE polarization, respectively. The symbols ε, μ, β, and λ are the permittivity, permeability, mode propagation constant, and wavelength, respectively, and $k_0 = 2\pi/\lambda$. Then we apply the continuity of the tangential electromagnetic components in the layer boundary to obtain the transfer matrix between each adjacent layer. Once the total transfer matrix $\mathbf{M}$ is established, the mode propagation constant β can be obtained by solving $|\mathbf{M}| = 0$. In the study, we focus on the effective refractive index $n_{\text{eff}} = \beta/k_0$. From the waveguide point of view, the real part of $n_{\text{eff}}(\text{Re}(n_{\text{eff}}))$ and the imaginary part of $n_{\text{eff}}(\text{Im}(n_{\text{eff}}))$ are involved with mode phase velocity and losses, respectively.

Figs. 1(a) and (b) show the calculated dispersion relations of TM- and TE-polarized OTSs, respectively. In both figures we divide the OTSs into two categories. One is called the propagating OTSs with $\text{Re}(n_{\text{eff}})$ to be much larger than $\text{Im}(n_{\text{eff}})$, which has already been reported before [9]. The other one is a non-propagating state as $\text{Im}(n_{\text{eff}})$ is much larger than $\text{Re}(n_{\text{eff}})$.

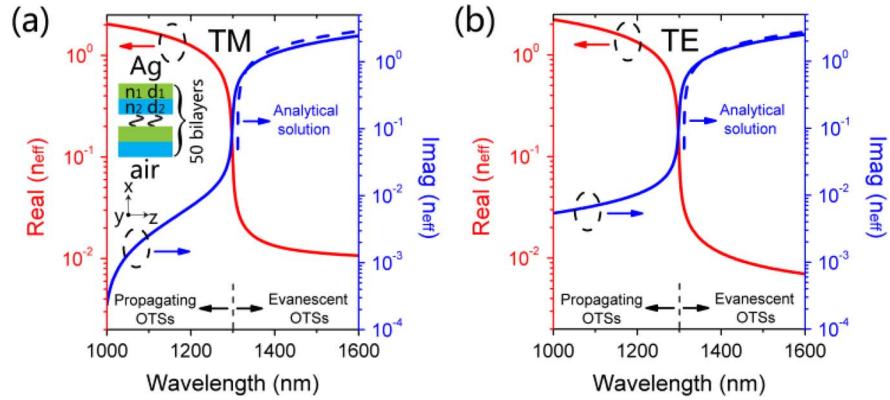

Fig. 1. Dispersion relations of (a) TM- and (b) TE-polarized OTSs at Ag-DBR interface. In each figure, the OTSs are divided into two categories as propagating OTSs and evanescent OTSs, respectively. The red solid and blue solid lines show the real part and imaginary part of the effective refractive index of the OTSs, respectively. The blue dashed lines represent the analytical solutions of the evanescent OTSs obtained by (6).

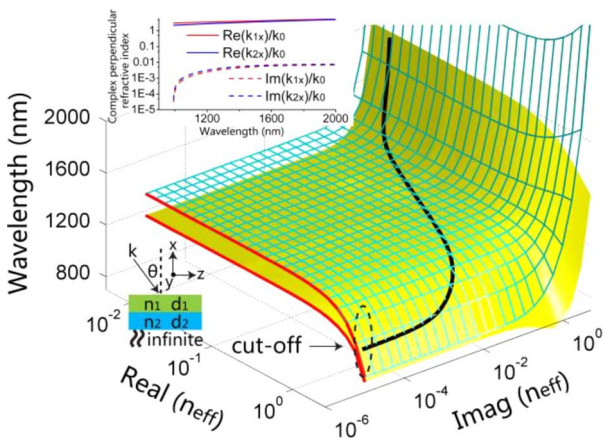

Fig. 2. Calculated TM-polarized Bragg forbidden band under complex propagation constants, where the yellow curved surface and the cyan mesh grid correspond to the two band edges, within which is the forbidden band. The black line shows the dispersion relation of TM-polarized OTSs at the Ag-DBR interface. The explanation of the inset can be referred to in the footnote at the bottom of the next column.

To the best of our knowledge, such non-propagating OTSs have not been reported before. We name the newly-found OTSs as evanescent OTSs as we will show that such states can be excited by evanescent waves.

B. Bragg Forbidden Band Under Complex Propagation Constants

To demonstrate the rationality of the evanescent OTSs, we calculate the Bragg forbidden band of the DBR structure, as OTSs should only exist within the forbidden band [9]. The schematic is shown in the inset of Fig. 2, where an incidence with wave number k and incident angle θ is launched on the DBR surface. The Bragg forbidden band depends on the tangential wave number $\beta = k \sin\theta = k_0 n_{\text{eff}}$. Therefore, n_{eff} is a real number or complex number in cases that the perpendicular wave number $k_x < k$ or $k_x > k$, respectively.

By following Yeh's theory, the Bragg forbidden band can be calculated by solving the well-known equation $|\cos K\Lambda| > 1$ [23].[1] The concrete expression is

$$\cos K\Lambda = \cos k_{1x} d_1 \cos k_{2x} d_2 - \frac{1}{2}\left[\frac{k_{1x}}{k_{2x}}\left(\frac{n_2}{n_1}\right)^{2s} + \frac{k_{2x}}{k_{1x}}\left(\frac{n_1}{n_2}\right)^{2s}\right] \times \sin k_{1x} d_1 \sin k_{2x} d_2 \quad (1)$$

where $k_{1x} = k_0(n_1^2 - n_{\text{eff}}^2)^{1/2}$, $k_{2x} = k_0(n_2^2 - n_{\text{eff}}^2)^{1/2}$, K is the Bloch wave number, and $s = 1$ or 0 for TM or TE polarization, respectively. Here we take TM polarization for instance, to study the first forbidden band. The results are shown in Fig. 2 by calculating under $\text{Re}(n_{\text{eff}})$ ranging from 0.005 to 2.5 and $\text{Im}(n_{\text{eff}})$ ranging from 10^{-5} to 5. The yellow curved surface and cyan mesh grid correspond to the two band edges, within which is the forbidden band. Conventionally, the forbidden band is considered only under real number of n_{eff} as shown by the region between the two red lines, where $\text{Im}(n_{\text{eff}})$ is so small ($\sim 10^{-5}$) that it can be ignored. As $\text{Re}(n_{\text{eff}})$ increases, the forbidden band shifts to blue. Interestingly, when we consider the forbidden band under complex n_{eff}, it shifts to red as $\text{Im}(n_{\text{eff}})$ increases. In Fig. 2, the black line shows the dispersion of TM-polarized OTSs at the Ag-DBR interface (Fig. 1(a)). The OTSs exist within the forbidden band all the time except the cut-off below 991 nm. Therefore, it can be concluded that the existence of the evanescent OTSs is a result of the extension of Bragg forbidden band under complex propagation constants.

The aforementioned shift of the forbidden band can be explained from the expression of Bloch wave number K in (1).

[1]It should be noted that as n_{eff} is a complex number, the Bloch wave number K is always a complex number no matter inside or outside the forbidden band. The definition of the forbidden band needs to be reconsidered. However, we still define the forbidden band as the region where $|\cos K\Lambda| > 1$, as we will show later that under the calculated n_{eff} of OTSs, the imaginary part of $\cos K\Lambda$ is always far less than its real part, thus the imaginary part of K is negligible within the allowed band where $|\cos K\Lambda| < 1$. It means the boundary between the forbidden band and the allowed band is still clear. This conclusion comes from the fact that k_{1x} and k_{2x} contribute to the imaginary part of $\cos K\Lambda$. It will be noted later from the inset of Fig. 2 that for all the n_{eff} of OTSs, k_{1x} and k_{2x} exhibit the negligible imaginary part far less than the real part.

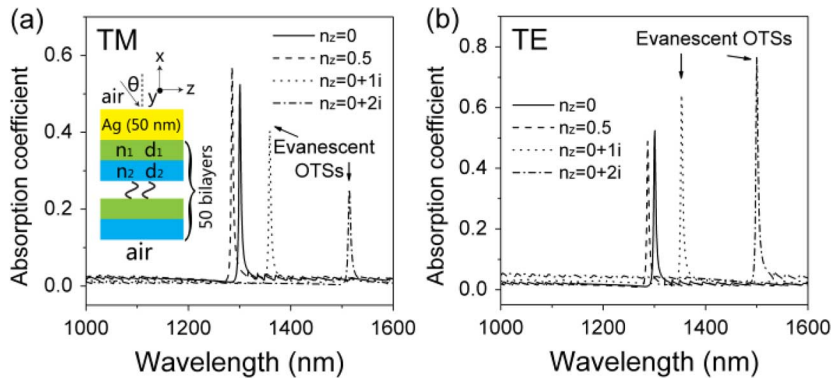

Fig. 3. Absorption spectra of the Ag-DBR structure with a 50 nm-thick Ag layer under different cases of incidence: $n_z = 0$ (solid line), 0.5 (dashed line), $0+1i$ (dotted line), and $0+2i$ (dash-dotted line) for (a) TM and (b) TE polarizations, respectively.

The Bragg wavelength λ_B corresponds to a wavelength exhibiting the maximum $|\cos K\Lambda|$, where both $k_{1x}d_1$ and $k_{2x}d_2$ are equal or close to $\pi/2$. Apparently, from the expressions of k_{1x} and k_{2x}, a longer wavelength is required with an increase in $\mathrm{Im}(n_{\mathrm{eff}})$ but a shorter wavelength is required with an increase in $\mathrm{Re}(n_{\mathrm{eff}})$, respectively. Then the forbidden band shifts as λ_B moves.

C. Analytical Solution of the Evanescent OTSs

We give an analytical solution of the discovered evanescent OTSs, by following the theory in [9]. The condition for the eigenmode of OTSs at a metal-DBR interface is

$$\phi(r_M r_{\mathrm{DBR}}) = 2N\pi \tag{2}$$

where N is an integer, ϕ demonstrates the phase, r_M is the amplitude reflection coefficient for the incidence on the metal from the medium with refractive index n_1, and r_{DBR} is the amplitude reflection coefficient for the incidence from the medium with refractive index n_1 on the DBR starting with a layer of the same refractive index n_1. Here we simply consider the evanescent OTSs with $n_{\mathrm{eff}} \approx 0 + n_i i$ and $n_i \ll n_1, n_2$. The reflection coefficient r_M can be derived from the Fresnel formula under evanescent waves as

$$r_M = (-1)^s \frac{(n_1/n_1')^{2s} n_1' - n_M}{(n_1/n_1')^{2s} n_1' + n_M} \tag{3}$$

where n_M is the refractive index of the metal, $n_1' = (n_1^2 + n_i^2)^{1/2}$ and we have used the approximation $n_M \approx (n_M^2 + n_i^2)^{1/2}$. The definition of s is the same as that in (1). By introducing the Drude model of the metal $n_M^2 = 1 - \omega_p^2/(\omega^2 + i\omega\gamma)$ and assuming γ is small and $\omega \ll \omega_p$, the reflection coefficient r_M can be derived as [9]

$$r_M \approx \exp(i[(1-s)\pi + 2(n_1/n_1')^{2s} n_1' \omega/\omega_p]) \tag{4}$$

where ω_p and γ are the plasma frequency and plasma collision rate fitted as $\omega_p = 1.1787 \times 10^{16}$ rad/s and $\gamma = 1.8550 \times 10^{14}$ rad/s for Ag, respectively, from the data extracted in Rsoft package [24]. Moreover, in the case $n_i \ll n_1, n_2$, we have $n_1' d_1 \approx n_2' d_2$, where $n_2' = (n_2^2 + n_i^2)^{1/2}$. Then the reflection coefficient r_{DBR} can be written as [25]

$$r_{\mathrm{DBR}} = \exp\left(i\left[(1-s)\pi + \frac{\pi n_1'(\omega - \omega_B)}{(n_1' - n_2')\omega_B}\right]\right) \tag{5}$$

where ω_B is the Bragg frequency by $\omega_B = \pi c/(2n_1' d_1)$ and c is the free space light speed. By substituting (4) and (5) into (2), the analytical solution of the evanescent OTSs frequency can be obtained as

$$\omega \approx \omega_B \left[1 + \frac{2n_1^{2s}(n_1' - n_2')\omega_B}{\pi n_1'^{2s}\omega_p}\right]^{-1} \tag{6}$$

Based on (6), the OTSs wavelengths are calculated under the range of n_{eff} from $0 + 0.05i$ to $0 + 3i$. The results are shown by blue dashed lines in Figs. 1(a) and (b). The analytical solutions match well with the exact solutions obtained by the waveguide mode theory based transfer matrix method.

D. Excitations of the Evanescent OTSs

Conventionally, the excitations of the propagating OTSs have been studied through the reflection spectra or absorption spectra under an outer incidence. To study the excitation method of the evanescent OTSs, we apply the transfer matrix method [25] to calculate the absorption spectra of the structure shown in the inset of Fig. 3(a). The incident light comes from air with z direction effective refractive index $n_z = k_z/k_0$, where k_z is the z direction wave number. Here we consider four conditions with $n_z = 0, 0.5, 0 + 1i$, and $0 + 2i$, respectively. It is noted that the cases of $n_z = 0$ and 0.5 correspond to the conditions under normal incidence and oblique incidence with $\theta = 30°$ in air, respectively, whereas the cases of $n_z = 0 + 1i$ and $0 + 2i$ correspond to the conditions under evanescent incidence with $k_x = \sqrt{2}k_0$ and $\sqrt{5}k_0$ in air, respectively. Here the evanescent incidence is only a mathematical abstraction, and we will discuss later how the evanescent OTSs can be excited physically. The absorption spectra are shown in Figs. 3(a) and (b) for TM and TE polarizations, respectively. We find that both the propagating OTSs ($n_z = 0$ and 0.5) and the evanescent OTSs ($n_z = 0+1i$ and $0+2i$) can be excited as shown by the absorption peaks. Therefore, we state that the evanescent OTSs can be

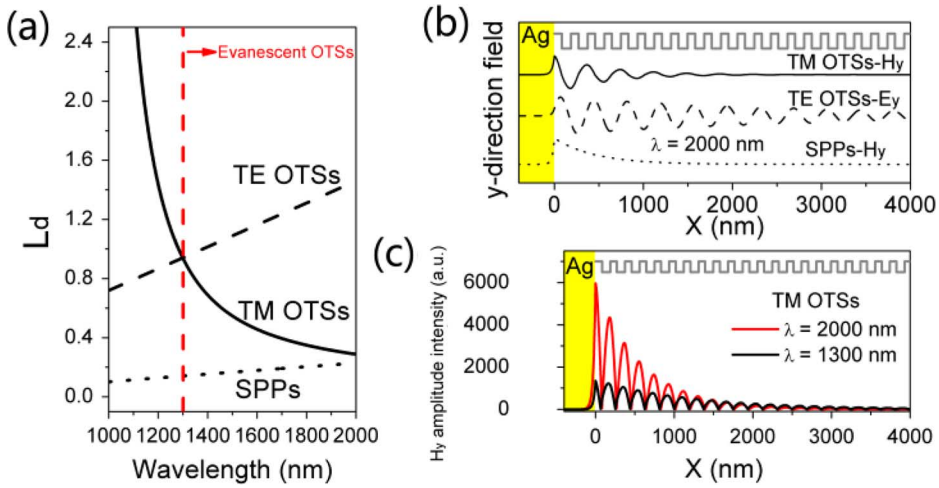

Fig. 4. (a) Normalized damping length of the SPPs (dotted line) at Ag-insulator interface, TM (solid line) and TE-polarized (dashed line) OTSs at Ag-DBR interface as a function of wavelength. (b) The y-direction field distributions with wavelength of 2000 nm for the three modes. (c) Normalized H_y amplitude intensity profiles of the TM-polarized OTSs with wavelengths of 1300 nm (black) and 2000 nm (red), respectively.

excited by z direction evanescent incidence with $n_z \approx n_{\text{eff}}$. As the OTSs at 1301 nm can be excited under $n_z = 0$, the boundary between the propagating OTSs and evanescent OTSs is defined as 1301 nm in Figs. 1(a) and (b).

We then discuss how to excite the aforementioned evanescent incidence physically. One possible method is to use evanescent waves generated by the total reflection from a medium with high refractive index to air. Such waves exhibit evanescent fields in the direction perpendicular to the medium-air interface. The evanescent OTSs can be excited if the wave numbers between the generated evanescent waves and the evanescent OTSs are matching. Another possible method is to apply the Fourier transform. To excite the evanescent OTSs with $n_{\text{eff}} \approx 0 + n_i i$, a field distribution of $\exp(-k_0 n_i z)$ is required. By applying the Fourier transform, such field distribution can be achieved via a combination of plane waves with amplitudes of $A(\beta_z) = \int_{-\infty}^{+\infty} \exp(-k_0 n_i |z|) \exp(-i\beta_z z)\, dz = (2k_0 n_i)/((k_0 n_i)^2 + \beta_z^2)$, where β_z is the z direction wave number of the plane wave. Such incidence is similar to the well-known Gaussian beam, and may be beneficial for the excitations of the evanescent OTSs. The aforementioned two methods both focus on the matching of the wave number, whereas radiative waves have also been used experimentally for the excitations of such evanescent states. In [26], evanescent photonic states with $\text{Im}(n_{\text{eff}})$ to be much larger than $\text{Re}(n_{\text{eff}})$ in an Ag-Si-Ag structure have been excited by integrating an optical source channel. Through the channel, the incidence has been coupled to radiative waves with fields being evanescent in the propagating direction. Then the evanescent photonic states can be excited by the generated radiative waves. Therefore, the evanescent OTSs studied here may also be excited by radiative waves which can be generated by a similar channel structure as that in [26].

E. Characteristics of the Evanescent OTSs

Then we study the localization characteristics of the OTSs by comparing with SPPs at an Ag-insulator interface. We define a damping refractive index n_d, by which the field in the DBR for OTSs or in the insulator for SPPs is damping as $\exp(-k_0 n_d x)$. Based on n_d, we introduce the normalized damping length $L_d = 1/(k_0 n_d \lambda) = 1/(2\pi n_d)$, corresponding to a normalized distance toward wavelength where the field intensity is 1/e of that at the interface. In fact this field is damping as $\exp[-\text{Im}(K)x]$ and $\exp[-k_0(n_{\text{SPPs}}^2 - n_2^2)^{1/2} x]$ for OTSs and SPPs, respectively, where the refractive index of the insulator is chosen as n_2, n_{SPPs} is the effective refractive index of the SPPs that can be calculated by $n_{\text{SPPs}} = [n_M^2 n_2^2/(n_M^2 + n_2^2)]^{1/2}$, and n_M is the refractive index of metal. We then have

$$L_{d,\text{OTSs}} = 1/(\lambda\, \text{Im}(K)),$$
$$L_{d,\text{SPPs}} = 1/\left[2\pi \left(n_{\text{SPPs}}^2 - n_2^2\right)^{1/2}\right] \quad (7)$$

Obviously, a mode with smaller L_d exhibits more strongly localized field distributions.

The results of the normalized damping length are shown in Fig. 4(a). It is noted that at around 1301 nm, TM- and TE-polarized OTSs exhibit the same localization characteristics but much worse than those of SPPs. However, as the wavelength increases, L_d decreases for TM-polarized OTSs but increases for TE-polarized OTSs. The opposite variation of L_d for TM- and TE-polarized OTSs is intrinsically due to the different eigenfunctions as shown in (1). The y-direction field distributions at the wavelength of 2000 nm for the three modes are shown in Fig. 4(b). We find that the field of TM-polarized evanescent OTSs is almost as strongly localized as that of SPPs. Although such field is upon sub-wavelength localizations, it is still more strongly localized than that of the propagating OTSs. Therefore, enhanced field intensity at the surface can be expected. Fig. 4(c) shows the normalized H_y amplitude intensity profiles of the TM-polarized OTSs with wavelengths of 1300 nm (black line) and 2000 nm (red line), respectively. We confirm that the TM-polarized evanescent OTSs with longer wavelength exhibit larger field intensity at the surface, which may be beneficial for surface-related applications.

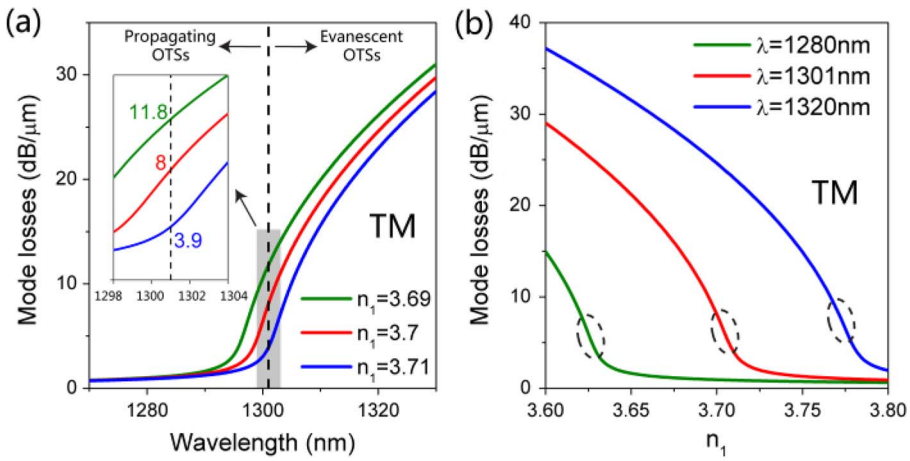

Fig. 5. (a) TM-polarized mode losses as a function of wavelength for different n_1. The dashed line corresponds the transition wavelength of 1301 nm for $n_1 = 3.7$. An enlarge view of the gray region is shown in the inset. (b) TM-polarized mode losses as a function of n_1 for different wavelengths.

F. Potential Applications of the Evanescent OTSs

Finally, we discuss the potential applications of evanescent OTSs. One potential application has already been discussed in the last sub-section that the TM-polarized evanescent OTSs may be beneficial for surface-related applications such as sensing. We focus on another application in the follows.

In Figs. 1(a) and (b), we find that a nearly vertical dispersion region exists around the transition wavelength ($\sim$1301 nm) between propagating OTSs and evanescent OTSs. Such nearly vertical dispersion suggests that the OTSs will be extremely sensitive to changes of n_1 and n_2. Modulation of the OTSs in this region can be expected, such as that achieved by a photonic mode in a similar dispersion region [26]. Here we discuss a modulation based on the mode losses, which can be calculated by $-10\lg(\exp[-\mathrm{Im}(n_{\mathrm{eff}})4\pi/\lambda])$. The TM-polarized results are shown in Fig. 5(a) for $n_1 = 3.69$ (green), 3.7 (red), and 3.71 (blue), which exhibit mode losses of 11.8 dB/μm, 8 dB/μm, and 3.9 dB/μm at the wavelength of 1301 nm, respectively. For instance, through a variation of 0.01 in n_1, a modulation depth of $\sim$4 dB can be achieved at a device length of only $\sim$1 μm. The variations of mode losses at different wavelengths are shown in Fig. 5(b). We find that the sensitive region in n_1 (dashed circles) can be adjusted by using different wavelengths. Therefore, the OTSs at the transition wavelength may be applied in absorption based modulators.

III. Conclusion

In summary, we have solved the eigenmodes of OTSs formed at the Ag-DBR interface and found a new type of OTSs named the evanescent OTSs. The existence of such states is attributed to the extension of Bragg forbidden band under complex propagation constants. Compared with the propagating OTSs, TM-polarized evanescent OTSs with longer wavelength exhibits more strongly localized field distributions associated with enhanced surface field intensity, which may be valuable for surface-related applications. Besides, another potential application as modulators is also discussed due to the nearly vertical dispersion of the OTSs at the transition wavelength.

Acknowledgment

The authors would like to thank Dr. X.-S. Luo (IME) and Dr. H.-F. Zhou (IME) for their valuable discussions.

References

[1] S. M. Tripathi, A. Kumar, E. Marin, and J. P. Meunier, "Highly sensitive miniaturized refractive index sensor based on Au-Ag surface gratings on a planar optical waveguide," *J. Lightw. Technol.*, vol. 28, no. 17, pp. 2469–2476, Sept. 2010.

[2] R. Zhang, B. B. Xu, X. Q. Liu, Y. L. Zhang, Y. Xu, Q. D. Chen, and H. B. Sun, "Highly efficient SERS test strips," *Chem. Commun.*, vol. 48, no. 47, pp. 5913–5915, Apr. 2012.

[3] H. Raether, *Surface Plasmons on Smooth and Rough Surfaces and on Gratings*. New York, NY, USA: Springer, 1988.

[4] Y. H. Su, Y. F. Ke, S. L. Cai, and Q. Y. Yao, "Surface plasmon resonance of layer-by-layer gold nanoparticles induced photoelectric current in environmentally-friendly plasmon-sensitized solar cell," *Light: Sci. Appl.*, vol. 1, no. 14, Jun. 2012.

[5] D. Lepage, A. Jiménez, J. Beauvais, and J. J. Dubowski, "Conic hyperspectral dispersion mapping applied to semiconductor plasmonics," *Light: Sci. Appl.*, vol. 1, no. 28, Sept. 2012.

[6] X. L. Zhang, J. Feng, J. F. Song, X. B. Li, and H. B. Sun, "Grating amplitude effect on electroluminescence enhancement of corrugated organic light-emitting devices," *Opt. Lett.*, vol. 36, no. 19, pp. 3915–3917, Oct. 2011.

[7] Y. Jin, J. Feng, X. L. Zhang, Y. G. Bi, Y. Bai, L. Chen, T. Lan, Y. F. Liu, Q. D. Chen, and H. B. Sun, "Solving efficiency-stability tradeoff in top-emitting organic light-emitting devices by employing periodically corrugated metallic cathode," *Adv. Mater.*, vol. 24, no. 9, pp. 1187–1191, Mar. 2012.

[8] G. Nemova and R. Kashyap, "A compact integrated planar-waveguide refractive-index sensor based on a corrugated metal grating," *J. Lightw. Technol.*, vol. 25, no. 8, pp. 2244–2250, Aug. 2007.

[9] M. Kaliteevski, I. Iorsh, S. Brand, R. A. Abram, J. M. Chamberlain, A. V. Kavokin, and I. A. Shelykh, "Tamm plasmon-polaritons: Possible electromagnetic states at the interface of a metal and a dielectric Bragg mirror," *Phys. Rev. B*, vol. 76, no. 16, pp. 165415-1–165415-5, Oct. 2007.

[10] M. E. Sasin, R. P. Seisyan, M. A. Kaliteevski, S. Brand, R. A. Abram, J. M. Chamberlain, I. V. Iorsh, I. A. Shelykh, A. Y. Egorov, A. P. Vasilev, V. S. Mikhrin, and A. V. Kavokin, "Tamm plasmon-polaritons: First experimental observation," *Superlattices Microstruct.*, vol. 47, no. 1, pp. 44–49, Jan. 2010.

[11] P. Yeh, A. Yariv, and A. Y. Cho, "Optical surface waves in periodic layered media," *Appl. Phys. Lett.*, vol. 32, no. 2, pp. 104–105, Jan. 1978.

[12] S. Brand, R. A. Abram, and M. A. Kaliteevski, "Tailor-made surface plasmon polaritons above the bulk plasma frequency: A design strategy for indium tin oxide," *J. Phys. D: Appl. Phys.*, vol. 43, no. 14, pp. 145104-1–145104-7, Mar. 2010.

[13] A. V. Kavokin, I. A. Shelykh, and G. Malpuech, "Lossless interface modes at the boundary between two periodic dielectric structures," *Phys. Rev. B*, vol. 72, no. 4, pp. 233102-1–233102-4, Dec. 2005.
[14] R. Brückner, M. Sudzius, S. I. Hintschich, H. Fröb, V. G. Lyssenko, and K. Leo, "Hybrid optical Tamm states in a planar dielectric microcavity," *Phys. Rev. B*, vol. 83, no. 3, pp. 033405-1–033405-4, Jan. 2011.
[15] M. Durach and A. Rusina, "Transforming Fabry-Pérot resonance into a Tamm mode," *Phys. Rev. B*, vol. 86, no. 23, pp. 235312-1–235312-6, Dec. 2012.
[16] I. Iorsh, P. V. Panicheva, I. A. Slovinskii, and M. A. Kaliteevski, "Coupled Tamm plasmons," *Tech. Phys. Lett.*, vol. 38, no. 4, pp. 351–353, Apr. 2012.
[17] O. Gazzano, S. M. Vasconcellos, K. Gauthron, C. Symonds, J. Bloch, P. Voisin, J. Bellessa, A. Lemaitre, and P. Senellart, "Evidence for confined Tamm plasmon modes under metallic microdisks and application to the control of spontaneous optical emission," *Phys. Rev. Lett.*, vol. 107, no. 24, pp. 247402-1–247402-5, Dec. 2011.
[18] C. Symonds, A. Lemaitre, E. Homeyer, J. C. Plenet, and J. Bellessa, "Emission of Tamm plasmon/exciton polaritons," *Appl. Phys. Lett.*, vol. 95, no. 15, pp. 151114-1–151114-3, Oct. 2009.
[19] E. Homeyer, C. Symonds, A. Lemaitre, J. C. Plenet, and J. Bellessa, "Strong coupling between Tamm plasmon and QW exciton," *Superlattices Microstruct.*, vol. 49, no. 3, pp. 224–228, Mar. 2011.
[20] X. L. Zhang, J. F. Song, X. B. Li, J. Feng, and H. B. Sun, "Optical Tamm states enhanced broad-band absorption of organic solar cells," *Appl. Phys. Lett.*, vol. 101, no. 24, pp. 243901-1–243901-5, Dec. 2012.
[21] J. Homola, *Surface Plasmon Resonance Based Sensor*. Berlin, Germany: Springer, 2006.
[22] D. Marcuse, *Theory of Dielectric Optical Waveguides*. New York, NY, USA: Academic, 1974.
[23] P. Yeh, A. Yariv, and C. S. Hong, "Electromagnetic propagation in periodic stratified media. I. General theory," *J. Opt. Soc. Amer.*, vol. 67, no. 4, pp. 423–438, Apr. 1977.
[24] FullWAVE, Rsoft Inc., Research Software [Online]. Available: http://www.rsoftinc.com
[25] P. Yeh, *Optical Waves in Layered Media*. New York, NY, USA: Wiley, 1988.
[26] J. A. Dionne, K. Diest, L. A. Sweatlock, and H. A. Atwater, "PlasMOStor: A metal-oxide-Si field effect plasmonic modulator," *Nano Lett.*, vol. 9, no. 2, pp. 897–902, Jan. 2009.

Xu-Lin Zhang received the B.S. degree in electronic information and science technology in 2009 from the College of Electronic Science and Engineering, Jilin University, China, where he is currently pursuing the Ph.D. degree. His current research interests are in the area of transformation optics based optoelectronics devices.

Jun-Feng Song received the B.S. and the Ph.D. degrees in 1993 and 2000, respectively, from the College of Electronic Science and Engineering, Jilin University, China. He was doing post-doctorate research in Changchun Institute of Optics, Chinese Academy of Sciences, Beijing, China, during 2000–2002.

He is now a Professor with Jilin University. His current research interests include silicon based optics devices, photonic crystal fibers, wavelength shifters.

Xian-Bin Li received the B.S. and the Ph.D. degrees in microelectronics in 2005 and 2010, respectively, from the College of Electronic Science and Engineering, Jilin University, China.

He is now a Lecturer in Jilin University. His research interests mainly focus on the key problems in microelectronics and optoelectronics with the first-principle calculation.

Jing Feng received the B.S. and the Ph.D. degrees in 1997 and 2003, respectively, from the College of Electronic Science and Engineering, Jilin University, China.

She worked as a Post-Doctoral Researcher in RIKEN, Japan, from 2003 to 2006. She is currently a Professor with Jilin University. Her current research interests include organic optoelectronics and optoelectronic devices.

Hong-Bo Sun received the B.S. and the Ph.D. degrees in electronics from Jilin University, Jilin, China, in 1992 and 1996, respectively.

He worked as a Postdoctoral Researcher in Satellite Venture Business Laboratory, the University of Tokushima, Japan, from 1996 to 2000, and then as an assistant professor in Department of Applied Physics, Osaka University, Osaka, Japan. In 2005, he was promoted as a Full Professor (Changjiang Scholar) in Jilin University, China. His current research interests are laser nanofabrication and ultrafast spectroscopy. By laser micronanofabrication technologies, various micro-optical, microelectronical, micromechanical, microoptoelectronic, microfluidic components and integrated systems have been produced, while the ultrafast dynamics solar cells, organic light-emitting devices and low-dimensional quantum systems have been deeply studied. So far, he has published over 100 scientific papers in the above field, which have been cited for more than 3500 times according to ISI search report.

Prof. Sun became a project leader under PRESTO (Precursory Research for Embryonic Science and Technology, Japan) program in 2001. He was awarded by Optical Science and Technology Society for his contribution to the technology of femtosecond laser initiated nanofabrication in 2002, and won Outstanding Young Scientist Award issued by the minister of MEXT (Ministry of Education, Culture, ports, Science & Technology, Japan) in 2006, and Wang Daheng Optics Award issued by China Optical Society, in 2009.